Pergamon

Int. J. Heat Mass Transfer. Vol. 37, No. 13, pp. 1925–1933, 1994

0017-9310/94 $7.00+0.00

0017-9310(94)E0026-Q

# The wall and free plumes above a horizontal line source in non-Darcian porous media

JIN-SHENG LEU and JIIN-YUH JANG†

Department of Mechanical Engineering, National Cheng-Kung University, Tainan, Taiwan 70101, Republic of China

(*Received* 5 *October* 1993)

**Abstract**—The natural convection flows from the wall and free plumes above a horizontal heat line source in a non-Darcian porous medium are investigated. The non-Darcian convective, boundary viscous and inertia effects are all considered. The results indicate that the non-Darcian effects decrease the peak velocities and increase the maximum temperatures, and thicken the temperature boundary layer. In addition, the wall plume has a lower peak velocity and a higher maximum temperature than the corresponding free plume. Moreover, solutions by using local similarity and local non-similarity methods overestimate the maximum temperature and peak velocity for both wall and free plume cases.

## 1. INTRODUCTION

THE steady buoyancy-induced flow arising from thermal energy sources is commonly referred to as a natural convection plume. Buoyancy sources, such as fires, electronic components, electrical heater and heated bodies, give rise to wake and develop into thermal plumes downstream. Among such plumes, two general types may be identified—the free plume and the wall plume. The free plume is typified by the buoyant flow above a heated horizontal wire or cylinder. A typical wall plume is the flow resulting from a line source of heat along the base of an adiabatic vertical plate. The free and wall plumes from a line or a point thermal source in a viscous fluid have been studied extensively (for example, refs. [1–5], and the references cited therein). However, the analogous problems of free and wall plumes in a saturated porous medium have received rather less attention. The applications include the natural convection cooling of buried electrical cables, the disposal of nuclear wastes, hot-wire anemometry, volcanic eruption, etc.

Wooding [6] developed a boundary-layer theory with an exact solution for steady-state natural convection from a line or point source in an infinite Darcian saturated porous medium (free plume). Lai [7] re-examined the same problem and obtained a closed form solution for a point source. Bejan [8] used a pertubation analysis to study the transient and steady natural convection from a point heat source at low Rayleigh number in a Darcian porous medium of infinite extent. The steady point heat sources at low and high Rayleigh numbers in an unbounded Darcian porous medium were investigated by Hickox and Watts [9] and Hickox [10]. Afzal and Salam [11] studied the natural convection arising from a point source in a Darcian porous medium bounded by an adiabatic conical surface. The Darcian mixed convection from a line thermal source imbedded at the leading edge of an adiabatic vertical surface (wall plume) in a saturated porous medium was numerically analyzed by Kumari *et al.* [12]. However, to the authors' knowledge, the non-Darican effects on the natural or mixed convection wall plume from a line source have not yet been investigated.

Coupled heat and mass transfer by natural convection at low Rayleigh number in an infinite Darcian porous medium has been reported by Poulikakos [13] for a point source, by Larson and Poulikakos [14] for a line source and by Lai and Kulacki [15] for a sphere. For a large Rayleigh number, Lai [16] obtained the similarity solution for a line source, and the closed form solutions are presented for the special case of Lewis number equal to 1.

All of the works mentioned above are based on the Darcy formulation. At a high Rayleigh number or in a high porosity medium, there is a departure from Darcy's law and the convective, boundary viscous, inertia and thermal dispersion effects not included in the Darcy model may become significant. Ingham [17] obtained an exact solution for the free convection from a line source in an unbounded non-Darican porous medium when only the inertia effect is considered, and he shows that the non-Darcian flow would produce a much more peaked temperature profile than that predicted by the Darcian flow. Local non-similarity solutions are reported by Lai [18] for natural convection from a line source to examine the inertia and thermal dispersion effects. It has been found that the inertial effect tends to reduce the flow and temperature profile while the thermal dispersion effect has enhanced this influence further. Cheng and

*Author to whom correspondence should be addressed.

## NOMENCLATURE

| | |
|---|---|
| $C$ | inertia coefficient |
| $C_p$ | specific heat of fluid |
| $Da_x$ | Darcy number, $K/x^2$ |
| $f$ | dimensionless stream function |
| $G$ | $\partial f/\partial\xi$ |
| $g$ | gravitational acceleration |
| $H$ | $\partial\theta/\partial\xi$ |
| $k$ | effective conductivity |
| $K$ | permeability |
| $Pr$ | Prandtl number, $\nu/\alpha_e$ |
| $Q$ | strength of thermal line source per unit length |
| $Ra_x$ | local Rayleigh number, $g\beta Qx^3/k\alpha_e\nu$ |
| $T$ | temperature |
| $u, v$ | volume averaged velocity in the $x$, $y$ directions |
| $x, y$ | axial and normal coordinates. |

Greek symbols

| | |
|---|---|
| $\alpha_e$ | effective thermal diffusivity |
| $\beta$ | coefficient of thermal expansion |
| $\Gamma$ | dimensionless inertia parameter, $K^{5/2}C^2g\beta Q/k\nu\alpha_e$ |
| $\varepsilon$ | porosity |
| $\xi$ | parameter, $1/(Da_x\,Ra_x^{2/5}) = (k\alpha_e\nu x^2/g\beta Q)^{2/5}/K$ |
| $\eta$ | pseudo similarity variable, $y(Ra_x)^{1/5}/x$ |
| $\theta$ | dimensionless temperature, $(Ra_x)^{1/5})(T(x,y)-T_\infty)k/Q$ |
| $\mu$ | fluid absolute dynamic viscosity |
| $\nu$ | fluid kinematic viscosity |
| $\rho$ | fluid density |
| $\Psi$ | stream function. |

Subscript

| | |
|---|---|
| $\infty$ | condition at the free stream. |

Zheng [19] used the local similarity method to study the mixed convection plume above a horizontal line source. The inertia and thermal dispersion effects are included. It is noted that numerical methods used in refs. [18, 19] such as local similarity method and local non-similarity method have their own drawbacks as the derivatives of certain terms are discarded in order to reduce the partial differential equations to ordinary differential equations. This has motivated the present investigation. The object is to give more accurate numerical solutions of the wall and free plumes due to line heat sources in a non-Darican porous medium. The governing partial differential equations are solved by using a suitable variable transformation and employing an efficient finite-difference Keller's Box method [20] incorporated with a numerical algorithm developed by Yu *et al.* [21] to deal with the integral boundary condition. The non-Darcian effects on the temperature and velocity fields will be examined in detail. In addition, both the local similarity and local non-similarity solutions are also presented in order to check the accuracy of these two approximate methods for the present problem.

## 2. MATHEMATICAL ANALYSIS

We consider the free convection from a horizontal line heat source, generating heat at a rate per unit length of $Q$, which is embedded in an unbounded porous medium (free plume) or embedded at the leading edge of an adiabatic vertical plate placed in a saturated porous medium (wall plume). The physical model and coordinate system for the wall and free plumes are illustrated in Fig. 1a and 1b, respectively. In order to study transport through non-Darcian media, the original Darcy model is improved by including convective, boundary viscous and inertia effects. In addition, we assume that: (1) the convective fluid and porous medium are in local thermal equilibrium; (2) the properties of the fluid except for the density term that is associated with the body force are constant; (3) variable porosity and thermal dispersion effects are neglected; and (4) the Boussinesq and boundary layer approximations are employed. Then, the governing equations become:

$$\frac{\partial u}{\partial x}+\frac{\partial v}{\partial y}=0, \tag{1}$$

$$\frac{\rho}{\varepsilon^2}\left(u\frac{\partial u}{\partial x}+v\frac{\partial u}{\partial y}\right)=\rho_\infty g\beta(T-T_\infty)-\frac{\mu}{K}u-\rho Cu^2+\frac{\mu}{\varepsilon}\frac{\partial^2 u}{\partial y^2}, \tag{2}$$

$$u\frac{\partial T}{\partial x}+v\frac{\partial T}{\partial y}=\alpha_e\frac{\partial^2 T}{\partial y^2}, \tag{3}$$

where $K$ is the permeability of the porous medium, $C$ is the transport property related to the inertia effect, $\varepsilon$ is porosity and $\alpha_e$ is the effective thermal diffusivity. The other symbols are defined in the Nomenclature.

The boundary conditions for equations (1)–(3) are:

(i) wall plume case:

$$x=0 \quad y>0 \quad u=0 \quad T=T_\infty$$

$$x>0 \quad y=0 \quad u=0 \quad v=0 \quad \frac{\partial T}{\partial y}=0$$

$$y=\infty \quad u=0 \quad T=T_\infty; \tag{4}$$

(ii) free plume case:

$$x=0 \quad y>0 \quad u=0 \quad T=T_\infty$$

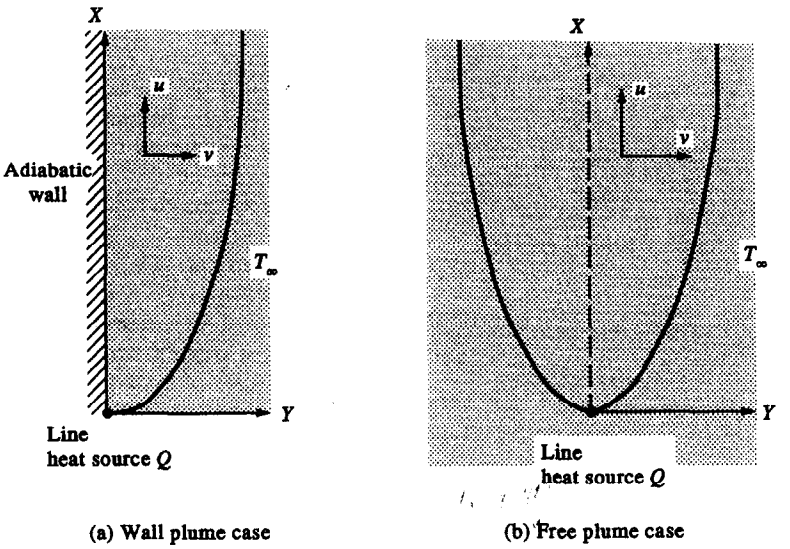


FIG. 1. The physical model and coordinate system.

$$x > 0 \quad y = 0 \quad \frac{\partial u}{\partial y} = 0 \quad v = 0 \quad \frac{\partial T}{\partial y} = 0$$

$$y = \infty \quad u = 0 \quad T = T_\infty. \tag{5}$$

It is noted that the major difference between the free plume and wall plume cases is the use of the no-slip boundary condition at the wall for a wall plume, as opposed to a plane of symmetry for a free plume. According to the principle of conservation of energy, the conservation of energy requires that, at any position $x > 0$, the convective energy is equal to the energy released by the line heat source, $Q$. Thus:

$$Q = \rho C_p \int_0^\infty u(T - T_\infty)\,\mathrm{d}y \quad \text{for wall plume,}$$

$$Q = \rho C_p \int_{-\infty}^{\infty} u(T - T_\infty)\,\mathrm{d}y \quad \text{for free plume.} \tag{6}$$

We introduce the following transformations:

$$\eta = \frac{y}{x}(Ra_x)^{1/5} \quad \xi = \xi(x)$$

$$f(\xi,\eta) = \frac{\Psi(x,y)}{\alpha_e (Ra_x)^{1/5}} \quad \theta(\xi,\eta) = \frac{T(x,y) - T_\infty}{Q/k}(Ra_x)^{1/5}, \tag{7}$$

where $Ra_x = g\beta Q x^3/k\alpha_e \nu$ is the local Rayleigh number and $\Psi$ is the stream function which automatically satisfies continuity equation (1). The coordinate $\xi$ is so chosen that $x$ does not appear explicitly in either the transformed governing equations or the transformed boundary conditions.

Substituting equation (7) into equations (1)–(3), we obtain:

$$\frac{1}{\varepsilon} f''' + \theta - \frac{1}{5\varepsilon^2 Pr}(f'^2 - 3ff'') - \xi f'$$

$$- \xi^{5/4}\frac{\Gamma^{1/2}}{Pr} f'^2 = \frac{4\xi}{5\varepsilon^2 Pr}\left(f'\frac{\partial f'}{\partial \xi} - f''\frac{\partial f}{\partial \xi}\right), \tag{8}$$

$$\theta'' + \frac{3}{5}(f'\theta + f\theta') = \frac{4}{5}\xi\left(f'\frac{\partial \theta}{\partial \xi} - \theta'\frac{\partial f}{\partial \xi}\right), \tag{9}$$

where primes denote partial differentiation with respect to $\eta$, $Pr = \nu/\alpha_e$ is the Prandtl number, $\Gamma = K^{5/2}C^2 g\beta Q/k\nu\alpha_e$ is the dimensionless inertia parameter expressing the relative importance of the inertia effect. $\xi$ is found to have the expression:

$$\xi(x) = \frac{1}{Da_x\, Ra_x^{2/5}} \propto \frac{x^{4/5}}{KQ^{2/5}}, \tag{10}$$

where $Da_x = K/x^2$ is the local Darcy number. The parameter $\xi$ characterizes the source strength ($Q$), the distance along the plate from the leading edge ($x$) and the permeability ($K$) of the porous medium. As $x$ increases or $Q$, $K$ decrease, the value of $\xi(x)$ increases. It is noted that Darcy's law corresponds to the case of $\xi \to \infty$ (i.e. $K \to 0$) with $\Gamma = 0$, for which the analytical solutions for the wall and free plumes can be obtained [6, 12]. For Darcy's law, the closed form solutions of the wall and free plumes in terms of the variables of the present study are as follows:

(i) wall plume case:

$$f' = 0.5\sqrt[3]{3}\,\xi^{-2/3}\,\mathrm{sech}^2\left(\frac{0.5}{\sqrt[3]{3}}\xi^{-1/3}\eta\right) \tag{11}$$

$$\theta = 0.5\sqrt[3]{3}\,\xi^{1/3}\,\mathrm{sech}^2\left(\frac{0.5}{\sqrt[3]{3}}\xi^{-1/3}\eta\right);$$

(ii) free plume case:

$$f' = 0.5\sqrt[3]{\tfrac{3}{4}}\xi^{-2/3}\,\mathrm{sech}^2\left(\frac{0.5}{\sqrt[3]{6}}\xi^{-1/3}\eta\right)$$

$$\theta = 0.5\sqrt[3]{\tfrac{3}{4}}\xi^{1/3}\,\mathrm{sech}^2\left(\frac{0.5}{\sqrt[3]{6}}\xi^{-1/3}\eta\right). \quad (12)$$

The transformed boundary conditions are:

(i) wall plume case:

$$f(\xi,0) = f'(\xi,0) = \theta'(\xi,0) = 0$$

$$f'(\xi,\infty) = \theta(\xi,\infty) = 0$$

$$\int_0^\infty f'\theta\,\mathrm{d}\eta = 1; \quad (13)$$

(ii) free plume case:

$$f(\xi,0) = f''(\xi,0) = \theta'(\xi,0) = 0$$

$$f'(\xi,\infty) = \theta(\xi,\infty) = 0$$

$$\int_0^\infty f'\theta\,\mathrm{d}\eta = \tfrac{1}{2}. \quad (14)$$

Because the condition $\theta(\xi,\infty) = 0$ is satisfied automatically by using the other conditions, the other five independent conditions in equations (13) and (14) are sufficient for solving the fifth-order partial differential governing equations (8) and (9). In terms of new variables, it can be shown that the dimensional velocity components and temperature are given by:

$$u = K^{1/4}\left(\frac{g\beta Q\alpha_c}{k\nu}\right)^{1/2}\xi^{1/4}f'(\xi,\eta)$$

$$v = \alpha_c K^{-1/2}\xi^{-1/2}\left(\frac{3}{5}f - \frac{2}{5}\eta f' + \frac{4}{5}\xi\frac{\partial f}{\partial\xi}\right)$$

$$T - T_\infty = K^{-3/4}\left(\frac{Q\nu\alpha_c}{g\beta k}\right)^{1/2}\xi^{-3/4}\theta(\xi,\eta). \quad (15)$$

## 3. NUMERICAL METHOD

Three different numerical methods—local similarity, local non-similarity and Keller's Box finite-difference methods—were used in the present study. Equations (8) and (9) associated with the boundary conditions (13) and (14) were solved by an efficient and accurate implicit finite-difference method similar to that described in Cebici and Bradshaw [20]. To begin with, the partial differential equations are first converted into a system of first-order equations, then these first-order equations are expressed in finite difference forms in terms of center difference. Denoting the mesh points in the $\xi$–$\eta$ plane by $\xi_i$ and $\eta_j$, where $i = 0, 1, \ldots, M$ and $j = 0, 1, \ldots, N$, this results in a set of non-linear difference equations for the unknowns at $\xi_i$ in terms of their values at $\xi_{i-1}$. The resulting non-linear finite difference equations are then solved by Newton's iterative method. The boundary layer equations are thus solved step by step by taking the converged solution at $\xi = \xi_{i-1}$.

We adopted the numerical algorithm [21] to deal with the integral constrains, equations (13) and (14). For the wall plume, we first drop the boundary conditions $f'(\xi,0) = 0$ and $\theta'(\xi,0) = 0$, and assume another two presupposed boundary conditions $f''(\xi,0) = s$ and $\theta(\xi,0) = t$, where $s$ and $t$ are the undetermined non-zero constants. The refined values of $s$ and $t$ can be estimated by Newton–Raphson method associated with two sets of variation equations which were derived by taking the derivatives of the finite-difference equations of equations (8) and (9) and their boundary condition (13) with respect to $s$ and $t$. The two sets of variation equations, due to retaining the tridiagonal block structure of the matrix, can be solved by using Keller's scheme. The two dropped boundary conditions together with the integral condition, equation (13), are treated as constraints. The iterations for adjusting the presupposed boundary conditions are repeated until the following criterion, which is the sum of squares of the discrepancies for the constrained conditions, is satisfied:

$$[f'(\xi,0)]^2 + [\theta'(\xi,0)]^2 + \left[\int_0^\infty f'\theta\,\mathrm{d}\eta - 1\right]^2 \leqslant \text{error (say, } 10^{-7}).$$

For free plume case, similar procedures are followed, except that the dropped boundary conditions $f'(\xi,0) = 0$ and $\theta'(\xi,0) = 0$ in the wall plume case are changed to $f''(\xi,0) = 0$ and $\theta'(\xi,0) = 0$ and two presupposed boundary conditions $f'(\xi,0) = s$ and $\theta(\xi,0) = t$ are assumed.

In the calculations, the values of $\eta_\infty = 20$ were found to be sufficiently accurate for $|f'_\infty| < 10^{-3}$. Uniform step sizes of $\Delta\eta = 0.05$ in the $\eta$-direction and $\Delta\xi = 0.1$ in the $\xi$-direction were used.

For the local similarity method, this problem consists of solving only equations (8) and (9) when the right-hand sides of these equations are replaced by zero. For the local non-similarity method, the governing equations at the second level of approximation are given by:

$$\frac{1}{\varepsilon}G''' + H - \frac{1}{5\varepsilon^2 Pr}(6f'G' - 7Gf'' - 3fG'') = \xi G' + f' + \xi^{1/4}\frac{\Gamma^{1/2}}{Pr}(\tfrac{5}{4}f'^2 + 2\xi f'G') + \frac{4\xi}{5\varepsilon^2 Pr}(G'^2 - GG''), \quad (16)$$

$$H'' + \tfrac{1}{5}(3fH' - f'H) + \tfrac{1}{5}(3G'\theta + 7G\theta') = \tfrac{4}{5}\xi(G'H - H'G), \quad (17)$$

where $G = \partial f/\partial\xi$ and $H = \partial\theta/\partial\xi$ are the auxiliary functions. The boundary conditions for the above two differential equations are:

Table 1. Three different solid–fluid combinations and heat source strength used in this study with $Pr = 5.4$

| Fluid | Solid | $d$ (mm) | $\varepsilon$ | $Q$ (W m$^{-1}$) | $K$ (m$^2$) | $C$ (m$^{-1}$) | $\Gamma$ |
|---|---|---|---|---|---|---|---|
| water | glass | 3 | 0.375 | 200 | $8\times10^{-9}$ | 6913 | 0.6 |
| water | glass | 6 | 0.4 | 200 | $4\times10^{-8}$ | 2836 | 6 |
| water | glass | 15 | 0.453 | 200 | $4.6\times10^{-7}$ | 686 | 160 |

(i) wall plume case:

$$G(\xi,0) = G'(\xi,0) = H'(\xi,0) = 0$$
$$G'(\xi,\infty) = 0$$
$$\int_0^\infty (G'\theta + f'H)\,d\eta = 0; \tag{18}$$

(ii) free plume case:

$$G(\xi,0) = G''(\xi,0) = H'(\xi,0) = 0$$
$$G'(\xi,\infty) = 0$$
$$\int_0^\infty (G'\theta + f'H)\,d\eta = 0. \tag{19}$$

A sixth-order variable step size Runge–Kutta integration routine in conjunction with the Newton–Raphson iterative scheme is used here to solve equations (8) and (9) for the local similarity solution, and equations (8) and (9) and (16) and (17) for the local non-similarity solution. The $\eta_\infty$ is decreased gradually with increasing $\xi$ and ranged from $\eta_\infty = 20$ for $\xi = 0$ to $\eta_\infty = 5$ for $\xi = 10$.

## 4. RESULTS AND DISCUSSIONS

Three different solid–fluid combinations listed in Table 1 are used in this study. The values of permeability $K$ and inertia coefficient $C$ are calculated by employing the Ergun model [22], $K = d^2\varepsilon^3/[150(1-\varepsilon)^2]$, $C = 1.75(1-\varepsilon)/\varepsilon^3 d$.

Figures 2 and 3 show the finite difference solutions of the velocity and temperature profiles across the boundary layer at different values of $\xi$ with $Pr = 5.4$, $\Gamma = 160$ for the wall plume and free plume, respectively. The velocity profiles are referred to the left and lower axes, while the temperature profiles are referred to the right and upper axes. The dashed lines denote the analytical solutions based on the Darcy model ($\xi = \infty$ and $\Gamma = 0$) [6, 12]. One can see that the velocity and temperature profiles for the wall and free plumes look similar except for the velocity near $\eta = 0$. For a free plume, because of the absence of wall at $\eta = 0$, the velocity should be symmetrical with $x$-axis. Thus, the maximum velocity occurs at $\eta = 0$, while, for a wall plume, at the wall $\eta = 0$ the velocity is zero because of the no-slip condition. It is also seen that the tangential peak velocity and maximum temperature decrease with increasing values of $\xi$; that is, both the tangential peak velocity and maximum temperature decrease with the increasing downstream distance $x$ for given source strength $Q$ and permeability $K$, or decrease with the decreasing $Q$ for fixed $x$ and $K$. In addition, the temperature boundary layer thicknesses for the wall and free plumes increase as $\xi$ increases. It is also observed that Darcy's solutions underpredict the maximum temperatures for the wall and free

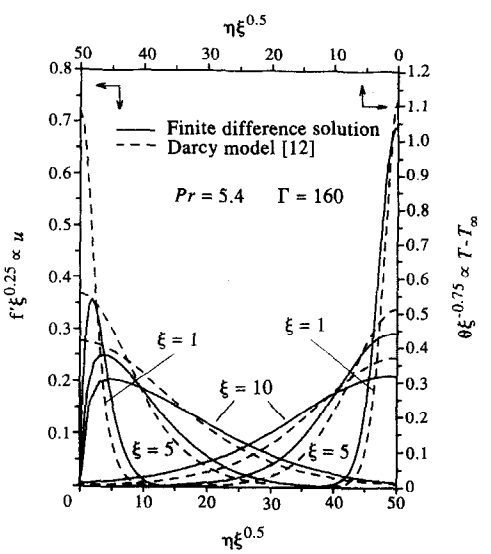


FIG. 2. The tangential velocity and temperature profiles at $\xi = 1$, 5 and 10 with $Pr = 5.4$, $\Gamma = 160$ for the wall plume.

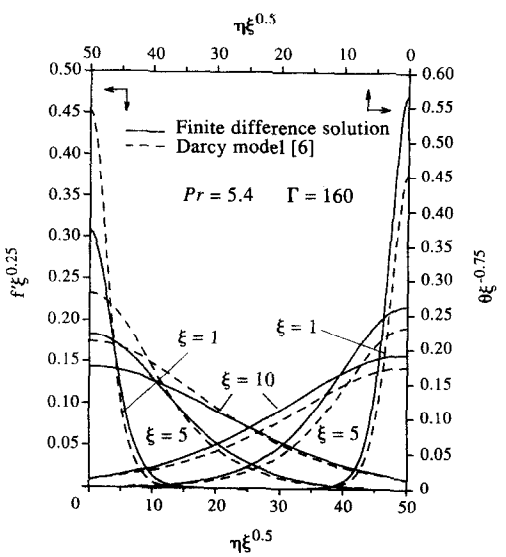


FIG. 3. The tangential velocity and temperature profiles at $\xi = 1$, 5 and 10 with $Pr = 5.4$, $\Gamma = 160$ for the free plume.

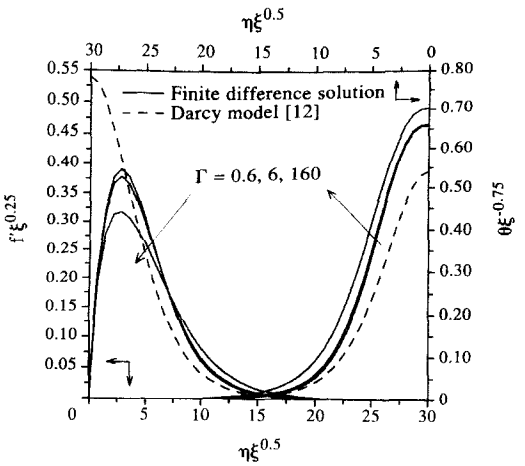


FIG. 4. The tangential velocity and temperature profiles for different values of $\Gamma = 0.6, 6, 160$ at $\xi = 2$ with $Pr = 5.4$ for the wall plume.

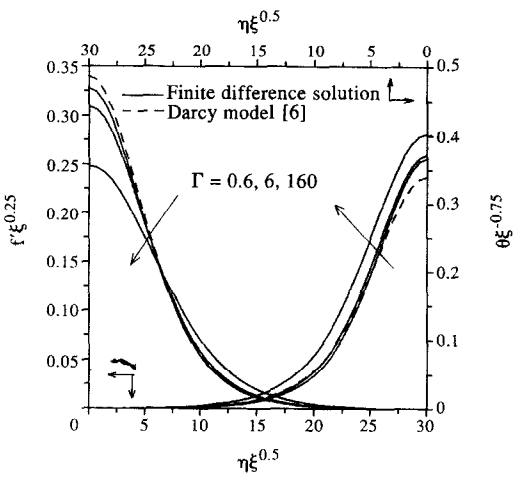


FIG. 5. The tangential velocity and temperature profiles for different values of $\Gamma = 0.6, 6, 160$ at $\xi = 2$ with $Pr = 5.4$ for the free plume.

plumes and, as would be expected, Darcy's law is only valid for large values of $\xi$.

Figures 4 and 5 show the finite difference solutions of the inertia effect ($\Gamma = 0.6, 6, 160$) on the tangential velocity and temperature profiles at $\xi = 2$ for the wall plume and free plume, respectively. The dash lines represent the Darcy model [6, 12]. It is seen that the inertia effect decreases the peak velocity and thicken the temperature boundary layer thickness. This is because the form drag of the porous medium is increased when the inertia effect is included.

Figures 6 and 7 shows the comparisons of the tangential velocity and temperature profiles, respectively, for the wall and free plumes calculated from the finite difference Keller's Box method and Darcy flow model [6, 12] at $\xi = 2.0$ with $\Gamma = 0$ (combined convective and boundary viscous effects, here called two effects) and $\Gamma = 160$ (combined convective, boundary viscous and inertia effects, here called three effects). The solid

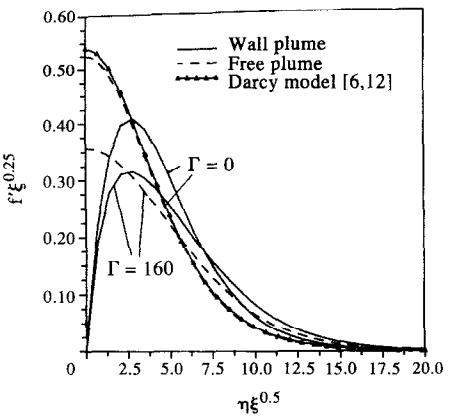


FIG. 6. Comparison of tangential velocity profiles for the wall and free plumes at $\xi = 2$ with $\Gamma = 0$ and 160.

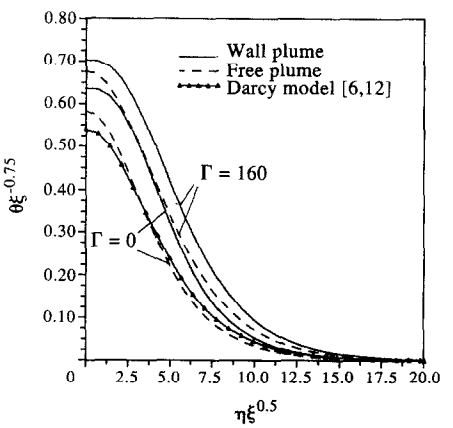


FIG. 7. Comparison of temperature profiles for the wall and free plumes at $\xi = 2$ with $\Gamma = 0$ and 160.

lines denote the wall plume solutions, while the dashed lines represent those for a free plume. In order to provide a common basis of comparison, the free plume results were corrected so that $Q$ represented the vertical flow of energy in the half-width of the free plume. It is noted that the Darcian solutions are the same for the wall and free plumes if the wall and the half-width of the free plumes have the same strength of heat source. It is seen that the wall plume has a lower peak velocity, a higher maximum temperature and a thicker temperature boundary layer thickness than the corresponding free plume. These differences are due to greater wall friction effect for a wall plume. Comparing the two effects ($\Gamma = 0$) with the three effects ($\Gamma = 160$), because of larger differences between curves of $\Gamma = 0$ and $\Gamma = 160$ for a free plume than for a wall plume, it is found that the inertia effect is more significant for the free plume. Moreover, compared with the solutions of the Darcy model with those of two effects ($\Gamma = 0$) for the wall and free plumes, one can see that boundary and convective effects are more important for a wall plume than for a free plume.

The maximum temperature (i.e. wall temperature for wall plume or center temperature for free plume)

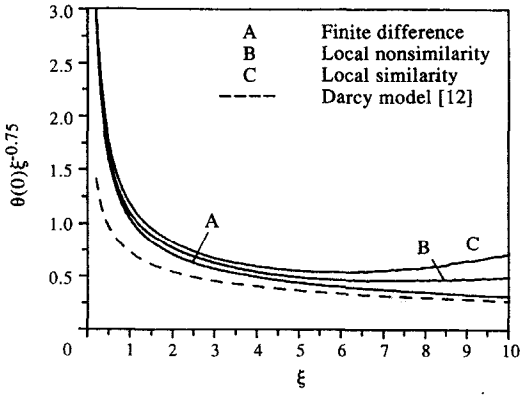


(a) Wall plume

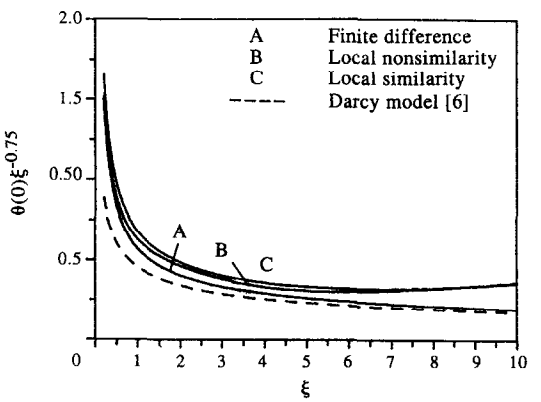


(b) Free plume

FIG. 8. The wall temperature and center temperature for the wall and free plumes over a wide range of $\xi$ with $Pr = 5.4$ and $\Gamma = 160$.

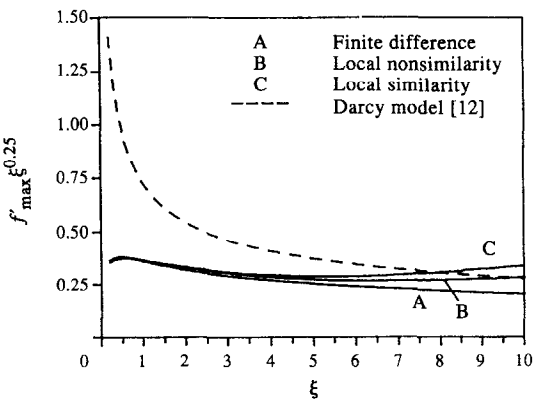


(a) Wall plume

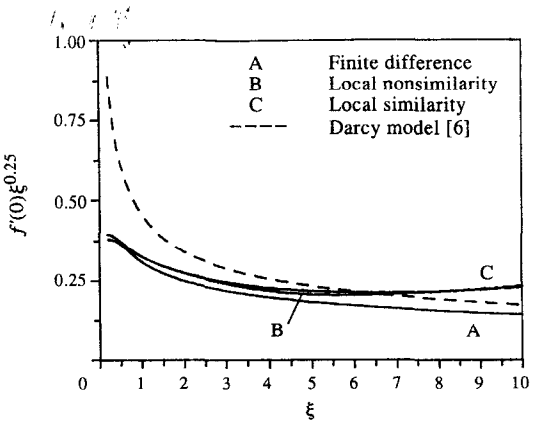


(b) Free plume

FIG. 9. The peak velocity for the wall and free plumes over a wide range of $\xi$ with $Pr = 5.4$ and $\Gamma = 160$.

and peak velocity over a wide range of $\xi$ are shown in Figs. 8 and 9, respectively, for $\Gamma = 160$. The local similarity, local non-similarity, finite difference and Darcy model [6, 12] solutions are presented. These solutions are also listed in Tables 2 and 3 for future reference. It is seen that both the local similarity and non-similarity methods overestimate the maximum temperature and peak velocity, while the Darcy model underestimates the maximum temperature and overestimates the peak velocity. As expected, the local non-similarity method yields more accurate results than those from the local similarity method. However, the agreement between the local non-similarity and Keller's Box methods of solution deteriorates when $\xi$ increases. For example, from Table 2 for the maximum temperature of the wall plume, the error for the local non-similarity method is 1% at $\xi = 0.2$ and 56.1% at $\xi = 10$, while for the local similarity method it is 4.8% at $\xi = 0.2$ and 125% at $\xi = 10$. For the free plume, the error for the local non-similarity method is 1.4% at $\xi = 0.2$ and 86.9% at $\xi = 10$, while for the local similarity method it is 10.2% at $\xi = 0.2$ and 88.1% at $\xi = 10$. In summary, for a maximum error of 10%, the local non-similarity method is found to be satisfactory for $\xi \leqslant 2$ (wall plume) and for $\xi \leqslant 1$ (free plume), respectively, while the local similarity method is satisfactory only for $\xi \leqslant 0.5$ (wall plume) and for $\xi \leqslant 0.2$ (free plume).

## 5. CONCLUSION

The numerical solutions for the natural convection flow from the wall and free plume above a horizontal heat line source in a non-Darcian porous medium are performed. A new parameter $\xi = 1/(Da_x Ra_x^{2.5}) = (k\alpha_e \nu x^2/g\beta Q)^{2.5}/K$ which characterizes the source strength ($Q$), the distance along the plate from the leading edge ($x$) and the permeability ($K$) of the porous medium is introduced, and Darcy's law corresponds to the case of $\xi \to \infty$. It is shown that the Darcy model underestimates the maximum temperature and overestimates the peak velocity. The numerical results also indicate that both the local similarity and non-similarity methods overpredict the maximum temperature and peak velocity. When compared with the Keller's Box method, for a largest error within 10%, the local non-similarity method is

Table 2. Values of $\theta(\xi,0)\ \xi^{-3/4}$ with various values of $\xi$ at $\Gamma = 160$ calculated based on the Darcy model, local similarity and local non-similarity and Keller's Box methods for the wall and free plumes, respectively. The percent errors of the former three approximate methods compared with the Keller's Box are also shown.

| | Wall plume | | | | | | |
|---|---|---|---|---|---|---|---|
| | Darcy | | Local similarity | | Local non-similarity | | Keller's Box |
| $\xi$ | $\theta(\xi,0)^*\ \xi^{-3/4}$ | % error | $\theta(\xi,0)^*\ \xi^{-3/4}$ | % error | $\theta(\xi,0)^*\ \xi^{-3/4}$ | % error | $\theta(\xi,0)\ \xi^{-3/4}$ |
| 0.2 | 1.4103 | 53.1 | 3.1489 | 4.8 | 3.0319 | 1.0 | 3.0021 |
| 0.5 | 0.9624 | 40.0 | 1.7571 | 9.6 | 1.6409 | 2.4 | 1.6031 |
| 1.0 | 0.7208 | 30.7 | 1.1790 | 13.4 | 1.0930 | 5.2 | 1.0393 |
| 2.0 | 0.5399 | 23.2 | 0.8180 | 16.4 | 0.7631 | 8.6 | 0.7027 |
| 3.0 | 0.4559 | 19.8 | 0.6694 | 17.7 | 0.6241 | 9.8 | 0.5687 |
| 5.0 | 0.3684 | 16.6 | 0.5539 | 25.5 | 0.4930 | 11.7 | 0.4415 |
| 7.0 | 0.3202 | 14.8 | 0.5547 | 47.5 | 0.4659 | 23.9 | 0.3760 |
| 8.0 | 0.3028 | 14.3 | 0.5929 | 67.9 | 0.4708 | 33.3 | 0.3532 |
| 10.0 | 0.2760 | 13.3 | 0.7158 | 125 | 0.4970 | 56.1 | 0.3183 |
| | Free plume | | | | | | |
| | Darcy | | Local similarity | | Local non-similarity | | Keller's Box |
| $\xi$ | $\theta(\xi,0)^*\ \xi^{-3/4}$ | % error | $\theta(\xi,0)^*\ \xi^{-3/4}$ | % error | $\theta(\xi,0)^*\ \xi^{-3/4}$ | % error | $\theta(\xi,0)\ \xi^{-3/4}$ |
| 0.2 | 0.8882 | 40.7 | 1.6525 | 10.2 | 1.5202 | 1.4 | 1.4991 |
| 0.5 | 0.6062 | 27.5 | 0.9708 | 16.1 | 0.8809 | 5.4 | 0.8361 |
| 1.0 | 0.4540 | 20.3 | 0.6771 | 18.9 | 0.6277 | 10.2 | 0.5694 |
| 2.0 | 0.3400 | 15.6 | 0.4838 | 20.1 | 0.4611 | 14.4 | 0.4029 |
| 3.0 | 0.2871 | 13.6 | 0.4024 | 21.1 | 0.3803 | 14.4 | 0.3324 |
| 5.0 | 0.2321 | 11.6 | 0.3335 | 30.0 | 0.3067 | 16.7 | 0.2627 |
| 7.0 | 0.2005 | 11.0 | 0.3218 | 42.8 | 0.3106 | 37.8 | 0.2254 |
| 8.0 | 0.1908 | 10.1 | 0.3273 | 54.2 | 0.3205 | 51.0 | 0.2123 |
| 10.0 | 0.1738 | 9.5 | 0.3613 | 88.1 | 0.3591 | 86.9 | 0.1921 |

Table 3. Values of $f'_{max}(\xi,\eta)\ \xi^{1/4}$ and $f'(\xi,0)\ \xi^{1/4}$ with various values of $\xi$ at $\Gamma = 160$ calculated based on the Darcy model, local similarity and local non-similarity and Keller's Box methods for the wall and free plumes, respectively. The percent errors of the former three approximate methods compared with the Keller's Box are also shown

| | Wall plume | | | | | | |
|---|---|---|---|---|---|---|---|
| | Darcy | | Local similarity | | Local non-similarity | | Keller's Box |
| $\xi$ | $f'_{max}(\xi,\eta)\ \xi^{1/4}$ | % error | $f'_{max}(\xi,\eta)\ \xi^{1/4}$ | % error | $f'_{max}(\xi,\eta)\ \xi^{1/4}$ | % error | $f'_{max}(\xi,\eta)\ \xi^{1/4}$ |
| 1.0 | 0.7208 | 101.1 | 0.3615 | 0.9 | 0.3642 | 1.6 | 0.3583 |
| 2.0 | 0.5399 | 70.6 | 0.3312 | 4.6 | 0.3289 | 4.0 | 0.3164 |
| 3.0 | 0.4559 | 58.5 | 0.3076 | 6.9 | 0.3025 | 5.1 | 0.2877 |
| 4.0 | 0.4043 | 51.4 | 0.2926 | 9.5 | 0.2825 | 5.7 | 0.2671 |
| 5.0 | 0.3684 | 46.7 | 0.2852 | 13.5 | 0.2708 | 7.8 | 0.2512 |
| 6.0 | 0.3414 | 43.1 | 0.2850 | 19.5 | 0.2657 | 11.4 | 0.2385 |
| 8.0 | 0.3028 | 38.3 | 0.3065 | 40.0 | 0.2701 | 23.3 | 0.2190 |
| 10.0 | 0.2760 | 34.9 | 0.3378 | 65.1 | 0.2822 | 37.9 | 0.2046 |
| | Free plume | | | | | | |
| | Darcy | | Local similarity | | Local non-similarity | | Keller's Box |
| $\xi$ | $f'(\xi,0)\ \xi^{1/4}$ | % error | $f'(\xi,0)\ \xi^{1/4}$ | % error | $f'(\xi,0)\ \xi^{1/4}$ | % error | $f'(\xi,0)\ \xi^{1/4}$ |
| 1.0 | 0.4540 | 47.3 | 0.3239 | 5.1 | 0.3252 | 5.5 | 0.3083 |
| 2.0 | 0.3400 | 36.9 | 0.2738 | 10.2 | 0.2721 | 9.5 | 0.2484 |
| 3.0 | 0.2871 | 32.1 | 0.2449 | 14.5 | 0.2393 | 10.1 | 0.2173 |
| 4.0 | 0.2547 | 29.2 | 0.2269 | 15.1 | 0.2167 | 9.8 | 0.1972 |
| 5.0 | 0.2321 | 27.0 | 0.2165 | 18.5 | 0.2056 | 12.5 | 0.1827 |
| 6.0 | 0.2151 | 25.3 | 0.2123 | 23.7 | 0.2039 | 18.8 | 0.1716 |
| 8.0 | 0.1908 | 22.9 | 0.2150 | 38.5 | 0.2131 | 37.3 | 0.1552 |
| 10.0 | 0.1738 | 21.2 | 0.2327 | 62.3 | 0.2306 | 62.1 | 0.1434 |

satisfactory for $\xi \leqslant 2$ for a wall plume and for $\xi \leqslant 1$ for a free plume, and the local similarity method is valid only for $\xi \leqslant 0.5$ for a wall plume and for $\xi \leqslant 0.2$ for a free plume. For the wall plume and free plume having the same vertical flow of energy in its half-width, it is shown that the wall plume has a lower peak velocity and a higher maximum temperature than the corresponding free plume.

## REFERENCES


1. T. Fujii, I. Morioka and H. Uehara, Buoyant plume above a horizontal line heat source, *Int. J. Heat Mass Transfer* **16,** 755–768 (1973).
2. J. A. Liburdy and G. M. Faeth, Theory of a steady laminar thermal plume along a vertical adiabatic wall, *Lett. Heat Mass Transfer*, **2,** 407–418 (1975).
3. E. M. Sparrow, S. V. Patankar and R. M. Abdel-Wahed, Development of wall and free plumes above a heated vertical plate, *J. Heat Transfer* **100,** 184–190 (1978).
4. K. V. Rao, B. F. Armaly and T. S. Chen, Analysis of laminar mixed convective plumes along vertical adiabatic surfaces, *J. Heat Transfer* **106,** 552–557 (1984).
5. H. T. Lin and J. J. Chen, Mixed convection wall plumes, *Int. J. Heat Mass Transfer* **30,** 1721–1726 (1987).
6. R. A. Wooding, Convection in a saturated porous medium at large Rayleigh number or Peclet number, *J. Fluid Mech.* **15,** 527–544 (1963)
7. F. C. Lai, Natural convection from a concentrated heat source in a saturated porous medium, *Int. Comm. Heat Mass Transfer* **17,** 791–800 (1990).
8. A. Bejan, Natural convection in an infinite porous medium with a concentrated heat source, *J. Fluid Mech.* **89,** 97–107 (1978).
9. C. E. Hickox and H. A. Watts, Steady thermal convection from a concentrated source in a porous medium, *J. Heat Transfer* **102,** 248–253 (1980).
10. C. E. Hickox, Thermal convection at low Rayleigh number from concentrated sources in porous medium, *J. Heat Transfer* **103,** 232–236 (1981).
11. N. Afzal and M. Y. Salam, Natural convection from point source embedded in Darcian porous medium, *Fluid Dynamic Res.* **6,** 175–184 (1990).
12. M. Kumari, I. Pop and G. Nath, Darcian mixed convection plumes along vertical adiabatic surfaces in a saturated porous medium, *Thermal Fluid Dynamic* **22,** 173–178 (1988).
13. D. Poulikakos, On bouyancy induced heat and mass transfer from a concentrated source in an infinite porous medium, *Int. J. Heat Mass Transfer* **28,** 621–629 (1985).
14. S. E. Larson and D. Poulikakos, Double diffusion from a horizontal line source in an infinite porous medium, *Int. J. Heat Mass Transfer* **29,** 492–495 (1986).
15. F. C. Lai and F. A. Kulacki, Coupled heat and mass transfer from a sphere buried in an infinite porous medium, *Int. J. Heat Mass Transfer* **33,** 209 (1990).
16. F. C. Lai, Coupled heat and mass transfer by natural convection from a horizontal line source in saturated porous medium, *Int. Comm. Heat Mass Transfer* **17,** 489–499 (1990).
17. D. B. Ingham, An exact solution for non-Darcy free convection from a horizontal line source of heat, *Thermal-Fluid Dynamic* **22,** 125–127 (1988).
18. F. C. Lai, Non-Darcy natural convection from a line source of heat in saturated porous medium, *Int. Comm. Heat Mass Transfer* **18,** 445–457 (1991).
19. P. Cheng and T. M. Zheng, Mixed convection in the thermal plume above a horizontal line source of heat in a porous medium of infinite extent, *Proceedings of 8th International Heat Transfer Conference* **5,** 2671–2675 (1986).
20. T. Cebici and P. Bradshaw, *Physical and Computational Aspects of Convective Heat Transfer*, Chapter 13. Springer, New York (1984).
21. W. S. Yu, H. T. Lin and H. C. Shih, Rigorous numerical solutions and correlations for two-dimensional laminar buoyant jets, *Int. J. Heat Mass Transfer* **35,** 1131–1141 (1992).
22. S. Ergun, Fluid flow through packed columns, *Chem. Eng. Progress* 89–94 (1952).